Combined System Identification and State Estimation for a Quadrotor UAV

Christoph Böhm[1], Christian Brommer[1], Alexander Hardt-Stremayr[1] and Stephan Weiss[1]

***Abstract*— Precise system identification is an important aspect of adequate control design and parameter definition to allow for accurate and reliable navigation. While this is well known in robotics, the community working with small rotorcraft Unmanned Aerial Vehicles (UAVs) has yet to discover the benefits. In contrast to existing work, which often performs offline or deterministic (i.e. closed-form) system identification, we present a probabilistic approach to the online estimation of system identification parameters and self-calibration states. Instead of decoupling system identification and state estimation for vehicle control, we merge the entire process into a holistic probabilistic framework to allow self-awareness and self-healing. Our observability analysis shows that most of the system identification parameters are observable and converge quickly to the optimal value using a combination of inertial cues, dynamic modeling, and an additional exteroceptive sensor. We support our theoretical findings with extensive tests simulating realistic data in Gazebo.**

I. Introduction

The increasing practical application of autonomous acting UAVs outside of controlled environments makes navigation-safety more relevant than ever. Important factors in safe navigation are self-awareness of the UAV, and the online estimation of states often assumed to be static and known. Such states include geometric and inertial properties. Exemplary geometric states are the relative poses of Inertial Measurement Unit (IMU) and exteroceptive sensors in the system's body frame, and typical inertial states are mass, the center of gravity, and the system's moments of inertia. These estimated properties used in model-based adaptive controls improve tracking performance, as shown by [2], [3].

We show that an extension of the system dynamics formulation with aerodynamic properties of the rotors, thrust coefficient and moment coefficient, allows the online estimation of before mentioned geometric, inertial, and aerodynamic properties. A further generalization of the formulation adds sensor frame rotations of IMU and exteroceptive sensors to account for arbitrary sensor placements. A successful (joint) estimation of all these properties is shown both in theory with a nonlinear observability analysis and in practice with realistic simulation experiments in Gazebo.

The proposed estimation for system identification and state estimation includes the following contributions:

[1] All authors are with the Control of Networked Systems Group at University of Klagenfurt, Austria. email: {firstname.lastname}@ieee.org

This research has received funding from the ARL within the BAA W911NF-12-R-0011 under grant agreement W911NF-16-2-0112 and from the Austrian Ministry for Transport, Innovation and Technology (BMVIT) under the grant agreement 878661 (SCAMPI)

Pre-print version, accepted Feb/2021, DOI follows ASAP ©IEEE.

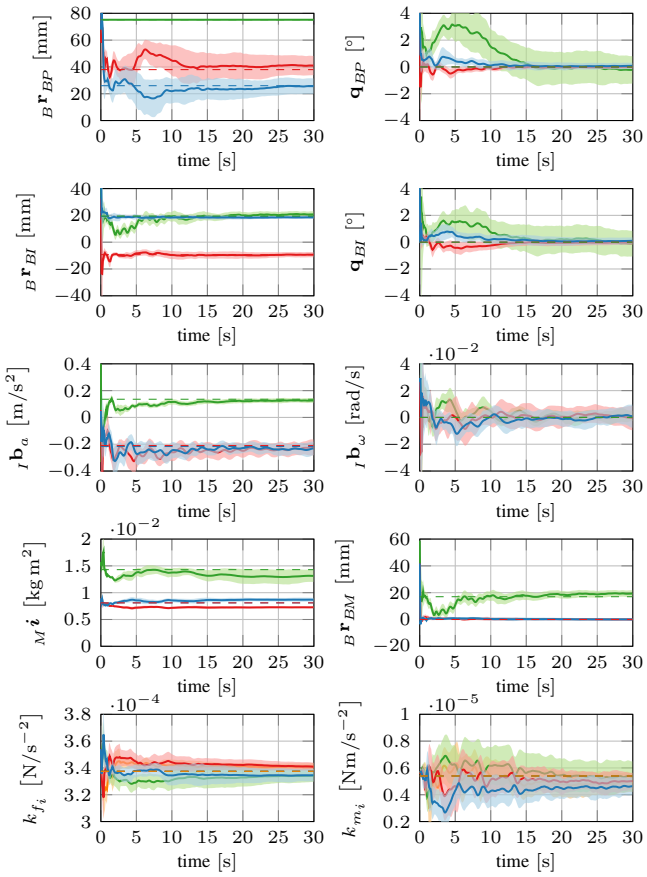

Fig. 1. Estimated geometric and inertial properties based on Lissajous trajectories [1]. Values assumed to be known (${}_B\mathbf{r}_{BP,z}$ and m) are not shown. Lines are the mean of the respective estimates over 30 runs. Axis x (blue), y (red), z (green) or rotor 1 (blue), 2 (red), 3 (green), 4 (orange). The shaded area represents the standard deviation of the estimates showing the spread. Dashed lines represent the ground truth values of the state.

- Extension of state-of-the-art system dynamics to include aerodynamic properties of the rotors k_{f_i} (thrust coefficient) and k_{m_i} (moment coefficient) within an estimation framework. Online estimation of these properties allows, e.g., detection of rotor failure during navigation.
- Addition of frame rotations of IMU and exteroceptive sensors with respect to the body frame $\mathbf{q}_{BP}$ and $\mathbf{q}_{BI}$, thus, making arbitrary placements of sensors possible.
- Observability analysis of the augmented system dynamics assuming pose and IMU measurements to determine observable and unobservable states as well as joint observable sub-spaces.
- Validation of observability analysis and estimation with experiments in Gazebo/RotorS.

II. Related Work

Trawny and Roumeliotis [4] used an IMU within an Indirect Kalman Filter (IKF) to propagate the pose of a body and an exteroceptive sensor to update the state values. This replacement simplifies the state estimator at the cost of information loss by neglecting the rotor speeds already available on the Flight Control Unit (FCU). Taking the system's dynamics itself to propagate the estimates and to use the IMU to update the estimate increases the overall information content. Furthermore, this work introduced unit quaternions as a singularity-free rotation representation in the context of Extended Kalman filter (EKF) based Visual Inertial Odometry (VIO). Kelly and Sukhatme [5] fused visual and inertial sensors based on the Unscented Kalman Filter (UKF) using system dynamics based on IMU measurements. However, calibration states between the camera and IMU together with intra-sensor calibration states, e.g., IMU biases, allow sensor self-calibration during run-time.

A detailed differential geometric analysis of the observability for the camera-IMU system was introduced by Hermann and Krener [6]. Krener and Ide [7] extended the observability analysis to calculate the quality of observability of states. These offline observability analysis insights can be used to generate specific motions that improve state observability and measurement quality. Observability-aware motion generation produces trajectories that aim to maximize the overall observability through the Expanded Empirical Local Observability Gramian (E^{2}LOG) introduced by Hausman et al. [8] and Preiss et al. [9].

Weiss [10], and Weiss and Siegwart [11] combined visual and inertial sensors inside an Iterated Extended Kalman Filter (IEKF) formulation on low-powered hardware. This approach allows online state estimation as well as sensor self-calibration. The system dynamics use the IMU measurements as input similar to previous methods. As others before, this approach lacks the capability of online identification of the underlying physical model.

Burri et al. [12], [13] applied self-calibration to geometric, inertial, and aerodynamic properties of a reduced rigid body model of a UAV. In contrast to this work, we allow an offset between IMU and the center of gravity and add the rotor thrust coefficients and moment coefficients to the estimation. These properties are estimated based on an offline Maximum Likelihood (ML) parameter identification. While nonlinear least-square algorithms produce more reliable results, the real-time application on-board the UAV becomes unfeasible with growing problem complexity and data stream length. The approach decouples these properties from the rest of the state vector, inherently neglecting correlations in the estimation process. In contrast, a filter-based approach can perform online on-board estimation in fixed time as it performs implicit marginalization.

Wuest et al. [1] formulated the estimation with the center of mass, the moments of inertia, and the weight of the UAV as a set of self-calibration states both for an EKF as well as an UKF. The individual rotor speeds serve as the input of the system's dynamics based on rigid body dynamics to propagate the state vector. An IMU and VIO based pose sensor provide information for state correction. Therefore, the UAV can perform tasks in the same quality even after a change of payload location. This influences the geometric and inertial properties of the UAV, changing its system response and rendering previous offline calibrations invalid. Böhm et al. [14] showed in combination with the E^{2}LOG that the convergence of geometric and inertial property estimates can be improved.

As Wuest et al. [1] uses assumptions on the alignment of the reference frames and, therefore, neglects self-calibration states like rotations between frames and the z-component of the IMU displacement, no full self-calibration is possible. Our work further reduces assumptions by allowing arbitrary sensor placement and the estimation of rotor related aerodynamic coefficients, hence, going towards a more generalized approach.

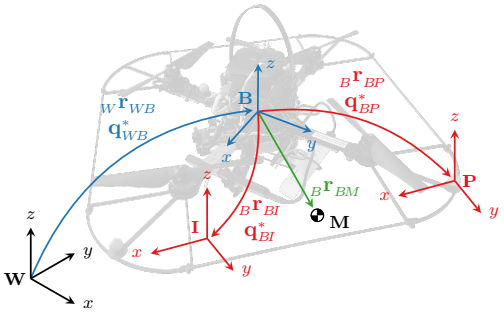

Fig. 2. Reference frames of the UAV model

III. Extended State Estimation for UAVs

To successfully calculate pose changes based on rotor speeds, one has to take into account mass, moments of inertia, the center of gravity, rotor thrust coefficients, and rotor moment coefficients. A continuous-time nonlinear state-space representation with underlying Newton-Euler equations describing rigid body dynamics formulates the system dynamics in the estimation. For ease of notation and readability, the time dependency of variables is neglected.

A. Notation

Leading subscripts indicate the reference frame of a variable. W is the fixed world frame, B is the UAV's body frame or the center of geometry, and M is the center of gravity. Sensors can be placed arbitrarily on the UAV, therefore we define two additional frames. P is the frame of the position or pose sensor, and I the IMU's frame. Fig. 2 illustrates the UAV's model reference frames. A position vector pointing from frame W to frame B, that is expressed in the coordinate frame W, is denoted by ${}_W\mathbf{r}_{WB}$ according to Eq. (1). This work uses quaternions to represent rotations and according to Solà [15] is the orientation of W with respect to B defined as $\mathbf{q}_{WB}$ as per Eq. (2).

$$ {}_{[Frame]}\mathbf{r}_{[From]\,[To]} \tag{1} $$

$$ \mathbf{q}_{[To]\,[From]} \tag{2} $$

The corresponding rotation matrix $\mathbf{R}_{WB}$ is a function of $\mathbf{q}_{WB}$. The rotation matrix is applied the following way ${}_W\mathbf{r}_{WB} = \mathbf{R}_{WB}\,{}_B\mathbf{r}_{WB}$. In addition, the conjugate of a quaternion is written as $\mathbf{q}^*_{WB}$ and corresponds to $\mathbf{R}^\mathsf{T}_{WB}$.

B. State Vector

The states ${}_W\mathbf{r}_{WB}$, ${}_W\mathbf{v}_{WB}$, and $\mathbf{q}_{WB}$ represent the position, linear velocity and orientation of B all expressed in and with respect to W. Similarly, ${}_B\boldsymbol{\omega}_{WB}$ denotes the angular velocity of B with respect to W and expressed in B.

$$\mathbf{x}_t = \left[{}_W\mathbf{r}^\mathsf{T}_{WB}, {}_W\mathbf{v}^\mathsf{T}_{WB}, \mathbf{q}^\mathsf{T}_{WB}, {}_B\boldsymbol{\omega}^\mathsf{T}_{WB}\right]^\mathsf{T} \tag{3}$$

To incorporate measurements from pose, position, or IMU sensors and allow full self-calibration, we include their position and orientation with respect to the UAV body frame B as states. Therefore, ${}_B\mathbf{r}_{BP}$ is the position of the sensor frame P expressed in and with respect to B. $\mathbf{q}_{BP}$ denotes the rotation quaternion of P in B. Continuing, ${}_B\mathbf{r}_{BI}$ denotes the position of the IMU frame I expressed in and with respect to B. $\mathbf{q}_{BI}$ denotes the rotation quaternion of I in B. ${}_I\mathbf{b}_a$ and ${}_I\mathbf{b}_\omega$ are the IMU's biases with ${}_I\mathbf{b}_a$ as linear acceleration bias and ${}_I\mathbf{b}_\omega$ as angular velocity bias. For further details regarding the body-IMU system dynamics (bias), we refer to Eq. (15) through Eq. (18).

$$\mathbf{x}_s = \left[{}_B\mathbf{r}^\mathsf{T}_{BP}, \mathbf{q}^\mathsf{T}_{BP}, {}_B\mathbf{r}^\mathsf{T}_{BI}, \mathbf{q}^\mathsf{T}_{BI}, {}_I\mathbf{b}^\mathsf{T}_a, {}_I\mathbf{b}^\mathsf{T}_\omega\right]^\mathsf{T} \tag{4}$$

The last part of the state vector contains the geometric, inertial, and aerodynamic properties of the UAV, i.e. system identification parameters. The mass of the UAV is denoted as m. The 3×3 inertia matrix of the UAV ${}_M\mathbf{I}$ is expressed with respect to M and its principal axes coincide with M. Therefore, only its diagonal elements ${}_M\boldsymbol{i}$ (moments of inertia) need to be represented in the state vector, ${}_M\mathbf{I} = \operatorname{diag}({}_M\boldsymbol{i})$. In addition, the frame B and M are aligned and $\mathbf{R}_{BM} \equiv \mathbf{I}$. This assumption is valid for our UAV configuration. The state ${}_B\mathbf{r}_{BM}$ expresses the position vector of M measured in, and relative to B, and describes the UAV's shift in the center of gravity. The coefficients for the thrust force and body torque of each rotor, k_{f_i} and k_{m_i}, are added to the state vector as well. These values are based on the squared motor speeds. This addition, compared to Wuest et al. [1], enables, e.g., rotor fault detection.

$$\mathbf{x}_p = \left[m, {}_M\boldsymbol{i}^\mathsf{T}, {}_B\mathbf{r}^\mathsf{T}_{BM}, k_{f_1}, \ldots, k_{f_n}, k_{m_1}, \ldots, k_{m_n}\right]^\mathsf{T} \tag{5}$$

Assuming the UAV is configured with 4 rotors, this results in a state vector with 48 elements.

$$\mathbf{x} = \left[\mathbf{x}^\mathsf{T}_t, \mathbf{x}^\mathsf{T}_s, \mathbf{x}^\mathsf{T}_p\right]^\mathsf{T}. \tag{6}$$

C. Control Inputs

The system control input is given as a set of angular velocities of the rotors ω_i in revolutions per second.

$$\mathbf{u} = \left[\omega_1, \ldots, \omega_N\right]^\top \tag{7}$$

Although this paper's UAV is a quadrotor with the number of rotors being $N = 4$, the system dynamics in this sections are applicable for different UAV configurations.

D. System Dynamics

A set of first-order time-dependent differential equations models the UAV's behavior based on current state $\mathbf{x}$, current control input $\mathbf{u}$, and process noise $\mathbf{w}$.

$$\dot{\mathbf{x}} = \mathbf{f}(\mathbf{x}, \mathbf{u}, \mathbf{w}) \tag{8}$$

As a first step, it is necessary to calculate the force ${}_B\mathbf{F}_t$ and torques ${}_B\mathbf{M}_t$ acting on the UAV. These are generated by the rotors with respect to the frame B or the center of gravity M respectively.

$${}_B\mathbf{F}_t = \sum_{i=1}^{N} {}_B\mathbf{F}_i \xrightarrow{\mathbf{R}_{BM}\equiv\mathbf{I}} {}_M\mathbf{F}_t = {}_B\mathbf{F}_t, \tag{9}$$

$$\text{where } {}_B\mathbf{F}_i = \mathbf{R}_{BR_i}\mathbf{e}_z k_{f_i}(\omega_i + \mathrm{w}_i)^2. \tag{10}$$

$$\xrightarrow[{}_B\mathbf{r}_{BM}\neq\mathbf{0}]{\mathbf{R}_{BM}\equiv\mathbf{I}} {}_M\mathbf{M}_t = \sum_{i=1}^{N} {}_B\mathbf{M}_i + \left[{}_B\mathbf{r}_{MR_i}\right]_\times {}_B\mathbf{F}_i, \tag{11}$$

$$\text{where } {}_B\mathbf{M}_i = \pm\mathbf{R}_{BR_i}\mathbf{e}_z k_{m_i}(\omega_i + \mathrm{w}_i)^2, \tag{12}$$

$$\text{and } {}_B\mathbf{r}_{MR_i} = {}_B\mathbf{r}_{BR_i} - {}_B\mathbf{r}_{BM}. \tag{13}$$

The mapping from rotor speeds to forces and torques relies on the following known constants: ${}_B\mathbf{r}_{BR_i}$ as the distance of the rotor to the body frame B, the orientation of the rotors $\mathbf{q}_{BR_i}$ in B, and a unit vector $\mathbf{e}_z = [0, 0, 1]^\mathsf{T}$. The rotors point upwards along the $+z$ axis of B and thus show no tilt resulting in $\mathbf{R}_{BR_i}(\mathbf{q}_{BR_i}) \equiv \mathbf{I}$. The noise $\mathrm{w}_i \sim \mathcal{N}(0, \sigma_i^2)$ refers to the uncertainty caused by the electronic speed controller (ESC). $[\bullet]_\times$ is the skew-symmetric matrix according to Solà [15].

From Newton-Euler equations with respect to the world frame W and a rigid body assumption, it is possible to derive the acceleration acting on any point of the UAV $\mathbf{a}_{act}(\mathbf{r})$ with respect to the center of mass.

$$\mathbf{a}_{act}(\mathbf{r}) = \left(\tfrac{1}{m}{}_B\mathbf{F}_t + \left[{}_B\dot{\boldsymbol{\omega}}_{WB}\right]_\times \mathbf{r} + \left[{}_B\boldsymbol{\omega}_{WB}\right]^2_\times \mathbf{r}\right) \tag{14}$$

This allows the formulation of the differential equations governing the state.

$${}_W\dot{\mathbf{r}}_{WB} = {}_W\mathbf{v}_{WB} \tag{15}$$

$${}_W\dot{\mathbf{v}}_{WB} = \mathbf{R}_{WB}\mathbf{a}_{act}(-{}_B\mathbf{r}_{BM}) - {}_W\boldsymbol{g} \tag{16}$$

$$\dot{\mathbf{q}}_{WB} = \tfrac{1}{2}\mathbf{q}_{WB} \otimes \left[0, {}_B\boldsymbol{\omega}^\mathsf{T}_{WB}\right]^\mathsf{T} \tag{17}$$

$${}_M\dot{\boldsymbol{\omega}}_{WB} = {}_M\mathbf{I}^{-1}\left({}_M\mathbf{M}_t - \left[{}_M\boldsymbol{\omega}_{WB}\right]_\times {}_M\mathbf{I}\ {}_M\boldsymbol{\omega}_{WB}\right) \tag{18}$$

$$\xrightarrow{\mathbf{R}_{BM}\equiv\mathbf{I}} {}_M\boldsymbol{\omega}_{WB} = {}_B\boldsymbol{\omega}_{WB} \tag{19}$$

Eq. (15) refers to the change in position. The change of linear velocity ${}_W\dot{\mathbf{v}}_{WB}$, Eq. (16), is a result of Euler and centrifugal forces of the rigid bodies movement, the control input's force ${}_B\mathbf{F}_t$, and ${}_W\boldsymbol{g} = [0, 0, 9.81]^\mathsf{T}$ as the gravitational pull acting on the UAV. Eq. (18) contains ${}_B\dot{\boldsymbol{\omega}}_{WB}$ and models its change with Euler's rotation equation around the center of gravity M including the control input's torque ${}_M\mathbf{M}_t$. ${}_I\dot{\mathbf{b}}_a$ and ${}_I\dot{\mathbf{b}}_\omega$ model the drift of the biases in form of a Brownian motion with $\mathbf{w}_{{}_I\mathbf{b}_a} \sim \mathcal{N}(0, \sigma^2_{{}_I\mathbf{b}_a})$ and $\mathbf{w}_{{}_I\mathbf{b}_\omega} \sim \mathcal{N}(0, \sigma^2_{{}_I\mathbf{b}_\omega})$, respectively. All other states are constant over time due to the rigid body assumption.

E. Measurement Models

State vector updates through pose, position, and IMU measurements are modeled based on the current state $\mathbf{x}$, control input $\mathbf{u}$, and measurement noise $\mathbf{v}$.

$$\mathbf{z} = \mathbf{h}(\mathbf{x}, \mathbf{u}, \mathbf{v}) \tag{20}$$

The sensor model $\mathbf{h}_{imu}$ of the IMU assumes a 6 degrees of freedom (DoF) sensor providing linear acceleration and angular velocity in 3 dimensions each. It is possible to predict the accelerations in frame I the same way as done for Eq. (16) with the displacement ${}_B\mathbf{r}_{MI}$, and the rotation $\mathbf{R}_{BI}^\mathsf{T}(\mathbf{q}_{BI}^*)$ taken into account. To predict the angular velocity one needs to rotate ${}_B\boldsymbol{\omega}_{WB}$ with $\mathbf{R}_{BI}^\mathsf{T}(\mathbf{q}_{BI}^*)$ into the frame I of the IMU. Both measurements are subject to bias ${}_I\mathbf{b}_a$ and ${}_I\mathbf{b}_\omega$ as well as noise $\mathbf{v}_a \sim \mathcal{N}(0, \sigma_a^2)$ and $\mathbf{v}_\omega \sim \mathcal{N}(0, \sigma_\omega^2)$.

$$\mathbf{h}_{imu} = \begin{bmatrix} \mathbf{R}_{BI}^\mathsf{T}\mathbf{a}_{act}({}_B\mathbf{r}_{MI}) + {}_I\mathbf{b}_a + \mathbf{v}_a \\ \mathbf{R}_{BI\,B}^\mathsf{T}\boldsymbol{\omega}_{WB} + {}_I\mathbf{b}_\omega + \mathbf{v}_\omega \end{bmatrix}, \tag{21}$$

$$\text{where } {}_B\mathbf{r}_{MI} = {}_B\mathbf{r}_{BI} - {}_B\mathbf{r}_{BM}. \tag{22}$$

A position sensor, e.g., a Global Positioning System (GPS) receiver, can provide absolute position information expressed in W, while a pose sensor, e.g., a tracking system, may provide absolute orientation information as well. The pose measurements $\mathbf{h}_{pose}$ can be predicted by moving the current pose of the body frame B into the sensor frame. Noises $\mathbf{v}_p \sim \mathcal{N}(0, \sigma_p^2)$ and $\mathbf{v}_\theta \sim \mathcal{N}(0, \sigma_\theta^2)$ depend on the sensor used and are assumed to be independent.

$$\mathbf{h}_{pose} = \begin{bmatrix} {}_W\mathbf{r}_{WB} + \mathbf{R}_{WB\,B}\mathbf{r}_{BP} + \mathbf{v}_p \\ \mathbf{q}_{WB} \otimes \mathbf{q}_{BP} \otimes \mathbf{v}_q \end{bmatrix}, \mathbf{v}_q = \begin{bmatrix} 1 \\ \frac{1}{2}\mathbf{v}_\theta \end{bmatrix} \tag{23}$$

IV. Nonlinear Observability Analysis

State estimation quality depends on how well different initial states $x(0)$ are distinguishable through the system's input-output map, also known as the system's observability.

A. Observability Analysis

Following the description for a nonlinear system in Hermann and Krener [6], stacking gradients of Lie derivatives ∇L_i^h gives us the observability matrix $\mathcal{O}$, as shown in Eq. (24). These Lie derivatives are based on the sensor model $\mathbf{h}(\mathbf{x}, \mathbf{u})$ and can be seen as $\mathbf{h}(\mathbf{x}, \mathbf{u})$ derived along $\mathbf{f}(\mathbf{x}, \mathbf{u})$. This connects measurements with state entries over the system dynamics.

$$\mathcal{O}(\mathbf{x}, \mathbf{u}) = \left[(\nabla L^0\mathbf{h})^\mathsf{T}, (\nabla L_{\mathbf{f}_0}^1\mathbf{h})^\mathsf{T}, (\nabla L_{\mathbf{f}_1}^1\mathbf{h})^\mathsf{T}, \dots \right]^\mathsf{T} \tag{24}$$

$$\text{with } L^0\mathbf{h} = \mathbf{h}(\mathbf{x}, \mathbf{u}) \text{ and } L_{\mathbf{f}}^i\mathbf{h} = \frac{\partial (L_{\mathbf{f}}^{i-1}\mathbf{h})}{\partial \mathbf{x}}\mathbf{f}(\mathbf{x}) \tag{25}$$

In the nonlinear system case, the matrix $\mathcal{O}$ depends on the current state values and control inputs, hence, the trajectory choice impacts the quality of observability. With motion that takes these facts into account it is possible to avoid unobservable directions and improve convergence [9]. In a fully observable system, the matrix $\mathcal{O}$ will have a full rank equal to the number of states in $\mathbf{x}$. To perform the observability analysis for our UAV, we create the control-affine form of the system dynamics from Sec. III-D, as suggested in Kelly and Sukhatme [5]. This control-affine form divides $\mathbf{f}(\mathbf{x}, \mathbf{u})$ into drift vector field $\mathbf{f}_0(\mathbf{x})$ and the control input vector fields of u_i as $\mathbf{f}_i(\mathbf{x})$, respectively.

$$\dot{\mathbf{x}} = \mathbf{f}_0 + \sum_{i=1}^{n} \mathbf{f}_i(\mathbf{x}) u_i^* \tag{26}$$

Note that there is a variable substitution u* for the squared rotor speeds in Eq. (10) and Eq. (12) as system inputs.

$$\mathbf{u}^* = [\omega_1^2, \dots, \omega_N^2]^\top \tag{27}$$

This step is necessary, because squared motor speeds will not allow the derivative of the control input vector fields $\mathbf{f}_i(\mathbf{x})$ which only depends on the state vector $\mathbf{x}$. By investigating the null-space of the observability matrix $\mathcal{O}$ and its spanning dimensions, one can identify observable and unobservable sub-spaces of a system's state space as well as jointly observable states through continuous symmetries as done by Martinelli [16]. Additional virtual measurements ensure the unit quaternion constraint holds for rotations.

$$\mathbf{h}_{unit} = \left[\mathbf{q}_{WB}^\mathsf{T}\mathbf{q}_{WB}, \mathbf{q}_{BP}^\mathsf{T}\mathbf{q}_{BP}, \mathbf{q}_{BI}^\mathsf{T}\mathbf{q}_{BI} \right]^\mathsf{T} \tag{28}$$

B. Discussion of Observability

The observability analysis of the presented approach assumes both pose and IMU measurements to be present. Tab. I shows the results of this analysis and gives us important insights, that can be used to interpret estimation results in the following section. It was conducted symbolically and numerically in Matlab, with the null-space calculations in numerical form.

The observability matrix $\mathcal{O}$ and its corresponding null-space show two joint observable sub-spaces and no unobservable states. These joint observabilities are *J1* (-1/8) and *J2* (-1/11) respectively. The positive values in brackets refer to the number of observable states, while the negative ones represent the unobservable states subtracted from the state vector length. *J1* includes one unobservable dimension spanned by the position of the UAV ${}_W\mathbf{r}_{WB}$, the velocity of the UAV ${}_W\mathbf{v}_{WB}$, and the z components of the displacement self-calibration states of the pose sensor ${}_B\mathbf{r}_{BP,z}$, the IMU ${}_B\mathbf{r}_{BI,z}$, and the center of gravity ${}_B\mathbf{r}_{BM,z}$. They get jointly observable due to Eq. (22) and the fact that ${}_B\mathbf{r}_{BM,z}$ gets no excitation from body torques in Eq. (12). ${}_W\mathbf{r}_{WB}$ and ${}_W\mathbf{v}_{WB}$ are part of this unobservable sub-spaces because a change of any calibration state can not be differentiated from positional or velocity changes. *J2* spans one unobservable dimension across the mass of the UAV m, the diagonal elements ${}_M\boldsymbol{i}$ of the UAV's inertia matrix, the rotor thrust coefficients k_{f_i}, and the rotor moment coefficients k_{m_i}. Those state components are on both sides of fractions in Eq. (16) and Eq. (18). Therefore, the system can only estimate the ratio between all these states. As mentioned before, all 27 remaining states are independently observable.

This gives us a rank of 46 compared to 48 dimensions. It is important to note, to get a fully observable system one needs to add a state component of each joint observable sub-space *J1* and *J2* as measurement to the estimation. This enforces application specific assumptions about the system.

TABLE I. Observability analysis results of the extended system model with pose & IMU measurements. The matrix $\mathcal{O}$ shows two jointly observable sub-spaces *J1* and *J2* including each one unobservable dimension with the other states being independently observable.

state vector dimension	observable dimensions	${}_W\mathbf{r}_{WB}$	${}_W\mathbf{v}_{WB}$	$\mathbf{q}_{WB}$	${}_B\boldsymbol{\omega}_{WB}$	${}_B\mathbf{r}_{BP}$		$\mathbf{q}_{BP}$	${}_B\mathbf{r}_{BI}$		$\mathbf{q}_{BI}$	${}_I\mathbf{b}_a$	${}_I\mathbf{b}_\omega$	m	${}_M\boldsymbol{i}$	${}_B\mathbf{r}_{BM}$		$k_{f_{1-4}}$	$k_{m_{1-4}}$
48	46	xyz:J1	xyz:J1	ok	ok	xy:ok	z:J1	ok	xy:ok	z:J1	ok	ok	ok	J2	J2	xy:ok	z:J1	J2	J2

V. Experimental Results

A. Simulation Setup

For this validation, a simulated UAV based on the AscTec Hummingbird UAV was used within the Gazebo/RotorS framework [17]. The benefit of such a realistic simulation environment is that most states are known (apart from the inertia matrix, which we calculated indirectly from other properties in the simulation). Noise and physics are modeled realistically, such that the evaluation of our estimator is best feasible. To prevent trajectory-based unobservability, we use the aggressively tuned, Model Predictive Control (MPC) in [18] to fly our trajectories with sufficient excitation in all 6 DoF. A well-tuned MPC can compensate small changes in the UAV's parameters, online estimates could improve robustness against larger changes.

The *Ground Truth* column of Tab. II lists all system properties modeled. The position and orientation values of sensor self-calibration parameters correspond to their placement on the UAV in Gazebo. The accelerometer bias ${}_I\mathbf{b}_a$ has been modeled based on a time series of IMU measurements from the real hardware IMU. The angular bias ${}_I\mathbf{b}_\omega$ is not applied as the FCU compensates it. All properties in $\mathbf{x}_p$ come from the AscTec Hummingbird model in RotorS. The elements of ${}_M\boldsymbol{i}$ are approximated from the RotorS definitions and may show some offset due to different modeled effects, e.g., moments of inertia calculations of the spinning rotors. Among the differences are velocity-induced drag forces and roll moments on the rotor, which are currently not considered in the model presented. For very fast flights, these effects are expected to impact the estimation process.

The control input's noise $\sigma_\mathbf{u}$ is 2 revolutions per second and was measured on the real hardware as an average of multiple time series of different rotor speed set-points. As mentioned in Sec. III-D, Brownian motion models the change of the IMU biases with $\sigma_{{}_I\mathbf{b}_a} = 8.3 \times 10^{-4}\,\mathrm{m}/\sqrt{\mathrm{s}^5}$ and $\sigma_{{}_I\mathbf{b}_\omega} = 1.3 \times 10^{-4}\,\mathrm{rad}/\sqrt{\mathrm{s}^3}$, respectively. In addition, the FCU's IMU measurement noise values are $\sigma_a = 0.083\,\mathrm{m/s^2}$ for the linear acceleration and $\sigma_\omega = 0.013\,\mathrm{rad/s}$ for the angular velocity. Position and orientation measurement noise of the pose sensor are $\sigma_p = 1 \times 10^{-3}\,\mathrm{m}$ and $\sigma_\theta = 1.7 \times 10^{-3}\,\mathrm{rad}$ assuming an absolute tracking system like OptiTrack. Each noise mentioned is assumed to be zero-mean gaussian white noise.

The frequency at which the FCU and/or Gazebo publish the motor speed values and IMU measurements is set to 200 Hz with pose measurements published at 50 Hz.

B. Evaluation of Performance

We tested the observability experimentally on 30 different trajectories to prevent trajectory-induced biases on the estimation results. As shown by Wuest et al. [1] and Böhm et al. [14], Lissajous figure based trajectories are a feasible way to excite all DoF to allow convergence of states. Each Lissajous trajectory lasts for 30 seconds, with a large amount of rotational movement along each axis to improve estimation performance. These Lissajous figures are generated at random by modulating the frequency component of each position axis as well as the yaw orientation. Fig. 3 depicts an example of such a Lissajous trajectory.

Estimation was performed in a fully observable configuration with ${}_B\mathbf{r}_{BP,z}$ and m assumed to be known and supplied as additional measurements (cf. discussion in Sec. IV-B). Because it is possible to place the pose sensor anywhere on the UAV (e.g., markers of a tracking system or a camera with VIO), its position can easily be measured with respect to the body frame B. The mass m can be determined by weighing the UAV before take-off. For all 30 runs, mean and standard deviation of the sensor state vector $\mathbf{x}_s$ and the system identification parameters state vector $\mathbf{x}_p$ have been calculated and can be seen in Fig. 1 for the assumed 4-rotor configuration. It shows the overall behavior of the estimation. The absolute error at the end of the 30 s flights compared to ground truth provides performance metrics indicating how well the estimates converge.

C. Discussion

Fig. 1 shows the estimation results of the sensor state vector $\mathbf{x}_s$, and the system identification parameters state vector $\mathbf{x}_p$ as mean with its spread over 30 runs. Trajectory state vector $\mathbf{x}_t$ entries are not part of this figure as each trajectory performs a different movement. It shows that each state converges fast towards the optimum, assuming ${}_B\mathbf{r}_{BP,z}$ and m are known, even when disregarding velocity-induced effects modelled in RotorS. This behavior confirms the theoretical observability results from Sec. IV-B. Tab. II shows the empirical results of the full state vector $\mathbf{x}$. For comparison, Wuest et al. [1] reach an absolute error below $0.22 \times 10^{-3}\,\mathrm{kg\,m^2}$ for the moments of inertia and less than 2 mm for the position of the center of gravity.

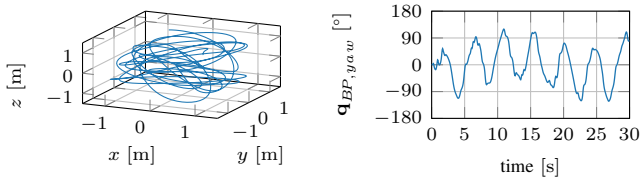

Fig. 3. Example of Lissajous trajectory with trajectory #12. The UAV position of the body frame ${}_B\,{}_W\mathbf{r}_{WB}$ (left) and its orientation around the z axis with respect to world frame ${}_W\,\mathbf{q}_{BP,yaw}$ (right).

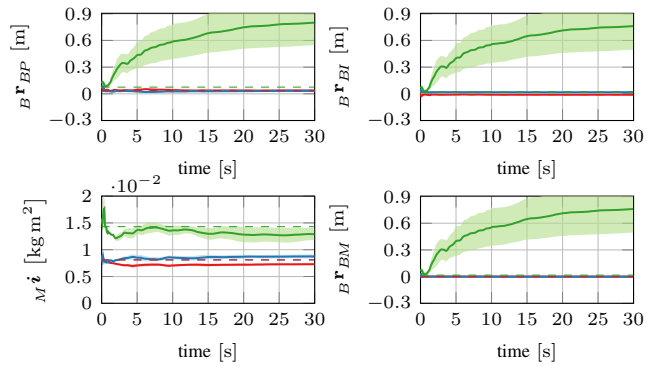

Fig. 4. Estimated geometric properties with m assumed to be known in the estimation. The one unobservable DoF of *J1* spanned by ${}_W\mathbf{r}_{WB}$, ${}_W\mathbf{v}_{WB}$, ${}_B\mathbf{r}_{BP,z}$, ${}_B\mathbf{r}_{BI,z}$, and ${}_B\mathbf{r}_{BM,z}$ results in a drift shared among all states. The state ${}_M\boldsymbol{i}$ becomes observable through the knowledge of m, included in *J2*. Lines are the mean of the respective estimates over 30 trails. Axis x (blue), y (red), z (green). The shaded area represents the standard deviation of the estimates showing the spread. Dashed lines represent the ground truth values of the respective state.

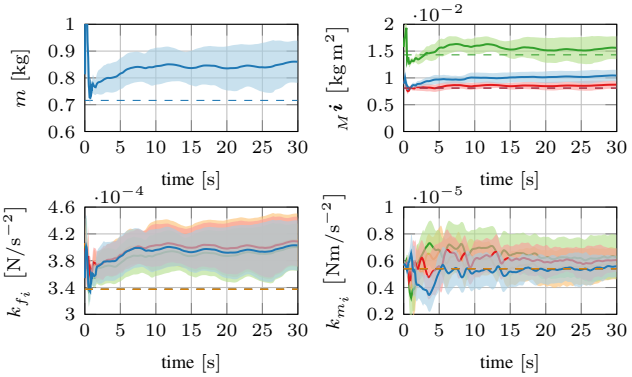

Fig. 5. Estimated inertial properties with assumed a-priory knowledge of self-calibration state ${}_B\mathbf{r}_{BP,z}$. The one unobservable dimension of *J2* gets spanned by all four depicted states and shows as overall drift of each states. Lines are the mean of the respective estimates over 30 trails. Axis x (blue), y (red), z (green) or rotor 1 (blue), 2 (red), 3 (green), 4 (orange). The shaded area represents the standard deviation of the estimates showing the spread. Dashed lines represent the ground truth values of the respective state.

TABLE II. Ground truth values and estimation results of the full state vector. The ground truth values of the trajectory states $\mathbf{x}_t$ are omitted as they change over time. The two jointly observable sub-spaces *J1* and *J2* get observable with the assumption that ${}_B\mathbf{r}_{BP,z}$ and m are known.

		Ground Truth	Absolute Error at the end	Standard Deviation at the end	Unit
${}_W\mathbf{r}_{WB}$	x	-	-0.5	12.7	mm
	y	-	3.9	14.6	
	z	-	-0.5	5.1	
${}_W\mathbf{v}_{WB}$	x	-	0.026	0.107	m/s
	y	-	0.051	0.107	
	z	-	0.004	0.033	
$\mathbf{q}_{WB}$	*roll*	-	-0.340	1.016	°
	pitch	-	0.158	1.007	
	yaw	-	0.128	1.798	
${}_B\boldsymbol{\omega}_{WB}$	x	-	-0.012	0.099	rad/s
	y	-	0.002	0.046	
	z	-	-0.006	0.152	
${}_B\mathbf{r}_{BP}$	x	26.0	-0.4	5.8	mm
	y	38.0	3.0	7.1	
	z	75.2	known	known	
$\mathbf{q}_{BP}$	*roll*	0.0	0.087	0.222	°
	pitch	0.0	-0.018	0.104	
	yaw	0.0	-0.224	1.016	
${}_B\mathbf{r}_{BI}$	x	19.0	-0.7	1.1	mm
	y	-9.3	-0.01	2.0	
	z	19.5	1.3	2.3	
$\mathbf{q}_{BI}$	*roll*	0.0	0.103	0.252	°
	pitch	0.0	-0.026	0.176	
	yaw	0.0	-0.115	0.953	
${}_I\mathbf{b}_a$	x	-0.22	-0.014	0.049	m/s^2
	y	-0.21	-0.015	0.058	
	z	0.14	-0.009	0.016	
${}_I\mathbf{b}_\omega$	x	0.0	0.001	0.009	rad/s
	y	0.0	-0.001	0.009	
	z	0.0	0.001	0.004	
m		0.716	known	known	kg
${}_M\boldsymbol{i}$	x	7.7×10^{-3}	0.6×10^{-3}	0.4×10^{-3}	kg m^2
	y	7.7×10^{-3}	-0.8×10^{-3}	0.2×10^{-3}	
	z	13.4×10^{-3}	-1.2×10^{-3}	1.1×10^{-3}	
${}_B\mathbf{r}_{BM}$	x	0.0	4.62×10^{-2}	0.7	mm
	y	0.0	3.61×10^{-2}	0.6	
	z	17.0	2.5	2.5	
k_{f_i}	1	3.375×10^{-4}	-0.030×10^{-4}	0.046×10^{-4}	N/s^{-2}
	2	3.375×10^{-4}	0.034×10^{-4}	0.030×10^{-4}	
	3	3.375×10^{-4}	-0.033×10^{-4}	0.046×10^{-4}	
	4	3.375×10^{-4}	0.035×10^{-4}	0.027×10^{-4}	
k_{m_i}	1	5.400×10^{-6}	-0.782×10^{-6}	0.680×10^{-6}	Nm/s^{-2}
	2	5.400×10^{-6}	-0.378×10^{-6}	0.637×10^{-6}	
	3	5.400×10^{-6}	-0.028×10^{-6}	1.142×10^{-6}	
	4	5.400×10^{-6}	-0.490×10^{-6}	0.720×10^{-6}	

In Sec. IV-B, two joint observabilities were discovered, *J1* and *J2*. Removing each assumption one by one during additional tests shows the validity of those claims. For *J1*, only m was set with a known value and for *J2*, ${}_B\mathbf{r}_{BP,z}$ was the only known value. Fig. 4 shows the development of *J1* over time. The position ${}_W\mathbf{r}_{WB}$ and the velocity ${}_W\mathbf{v}_{WB}$ of the UAV, as well as the self-calibration states ${}_B\mathbf{r}_{BP,z}$, ${}_B\mathbf{r}_{BI,z}$, and ${}_B\mathbf{r}_{BM,z}$ do not converge and drift away from the ground truth values jointly, corresponding to the one unobservable dimension. This indicates that the z axis of the body frame B can be chosen freely. The state ${}_M\boldsymbol{i}$ shows that *J2* is independent of *J1*. Fig. 5 shows case *J2* in which the mass of the UAV is not known, but ${}_B\mathbf{r}_{BP,z}$ is. All affected states, the mass m, the moments of inertia ${}_M\boldsymbol{i}$, the thrust coefficients k_{f_i}, and the moment coefficients k_{m_i}, show the same drift behavior similar to the previous case. Also, the shared drift corresponds to the one unobservable dimension of *J2*.

VI. Conclusion

We have shown that self-awareness and online self-calibration of an UAV is possible through state estimation of geometric, inertial, and aerodynamic properties of the UAV, given only two a-priori values. This method is more reliable than using offline calibration methods as system changes during task execution can invalidate their results after calibration. We include thrust coefficients (k_{f_i}) and moment coefficients (k_{m_i}) of each rotor as well as frame rotations of IMU ($\mathbf{q}_{BI}$) and exteroceptive sensors ($\mathbf{q}_{BP}$) with respect to the body frame. These estimates provide improved information on different levels of control compared to both offline calibration and currently used system simplifications. For example, short-term planning of a MPC can improve with a better approximation of possibly changing values, and-long term planning of an autonomous operating swarm can enhance the monitoring of an individual agent's health (e.g., detection of rotor failure). Empirical results confirm our understanding of the theoretical nonlinear observability analysis. This analysis, assuming pose and IMU measurements, revealed two joint observable sub-spaces, each spanning one unobservable dimension. Applying only two assumptions (e.g., ${}_B\mathbf{r}_{BP,z}$ and m are known) renders the whole state vector observable due to their joint inter-linkage.

REFERENCES

[1] V. Wuest, V. Kumar, and G. Loianno, "Online Estimation of Geometric and inertia parameters for multirotor aerial vehicles," in *IEEE International Conference on Robotics and Automation (ICRA)*, May 2019.

[2] A. L'Afflitto, R. B. Anderson, and K. Mohammadi, "An Introduction to Nonlinear Robust Control for Unmanned Quadrotor Aircraft: How to Design Control Algorithms for Quadrotors Using Sliding Mode Control and Adaptive Control Techniques [Focus on Education]," *IEEE Control Systems Magazine (CS-M)*, vol. 38, no. 3, pp. 102–121, June 2018.

[3] M. W. Achtelik, S. Lynen, M. Chli, and R. Siegwart, "Inversion Based Direct Position Control and Trajectory Following for Micro Aerial Vehicles," in *2013 IEEE/RSJ International Conference on Intelligent Robots and Systems (IROS)*, Nov 2013, pp. 2933–2939.

[4] N. Trawny and S. I. Roumeliotis, "Indirect Kalman Filter for 3D Attitude Estimation," CS&E, Technical Report 2005-002, 2005. [Online]. Available: https://pdfs.semanticscholar.org/7d78/9dd851ccf6100a3045ab9347b35eb86a9106.pdf

[5] J. Kelly and G. S. Sukhatme, "Visual-Inertial Sensor Fusion: Localization, Mapping and Sensor-to-Sensor Self-Calibration," *The International Journal of Robotics Research (IJRR)*, vol. 30, no. 1, pp. 56–79, 2011.

[6] R. Hermann and A. Krener, "Nonlinear Controllability and Observability," *IEEE Transactions on Automatic Control (TAC)*, vol. 22, no. 5, pp. 728–740, October 1977.

[7] A. J. Krener and K. Ide, "Measures of Unobservability," in *Proceedings of the 48h IEEE Conference on Decision and Control (CDC)*, Dec 2009, pp. 6401–6406.

[8] K. Hausman, J. Preiss, G. S. Sukhatme, and S. Weiss, "Observability-Aware Trajectory Optimization for Self-Calibration With Application to UAVs," *IEEE Robotics and Automation Letters (RA-L)*, vol. 2, no. 3, pp. 1770–1777, July 2017.

[9] J. A. Preiss, K. Hausman, G. S. Sukhatme, and S. Weiss, "Simultaneous self-calibration and navigation using trajectory optimization," *The International Journal of Robotics Research (IJRR)*, vol. 37, no. 13-14, pp. 1573–1594, 2018.

[10] S. Weiss, "Vision Based Navigation for Micro Helicopters," Ph.D. dissertation, ETH Zurich, 2012. [Online]. Available: https://www.research-collection.ethz.ch/bitstream/handle/20.500.11850/52698/eth-5889-02.pdf

[11] S. Weiss and R. Siegwart, "Real-Time Metric State Estimation for Modular Vision-Inertial Systems," in *2011 IEEE International Conference on Robotics and Automation (ICRA)*, May 2011, pp. 4531–4537.

[12] M. Burri, J. Nikolic, H. Oleynikova, M. W. Achtelik, and R. Siegwart, "Maximum Likelihood Parameter Identification for MAVs," in *2016 IEEE International Conference on Robotics and Automation (ICRA)*, May 2016, pp. 4297–4303.

[13] M. Burri, M. Bloesch, Z. Taylor, R. Siegwart, and J. Nieto, "A framework for maximum likelihood parameter identification applied on MAVs," *Journal of Field Robotics (JFR)*, vol. 35, no. 1, pp. 5–22, 2018.

[14] C. Böhm, G. Li, G. Loianno, and S. Weiss. (2020) Observability-Aware Trajectories for Geometric and Inertial Self-Calibration. [Online]. Available: https://drive.google.com/file/d/1_O14-7iBh3nlwmOC4q7QrdcskQHocKOX/view

[15] J. Solà, "Quaternion kinematics for the error-state Kalman filter," *arXiv e-prints*, Nov. 2017.

[16] A. Martinelli, "Continuous Symmetries and Observability Properties in Autonomous Navigation," INRIA, Research Report RR-7049, 2010. [Online]. Available: https://hal.inria.fr/inria-00421233

[17] F. Furrer, M. Burri, M. Achtelik, and R. Siegwart, "RotorS - A modular gazebo MAV simulator framework," in *Robot Operating System (ROS)*. Springer, 2016, pp. 595–625.

[18] M. Kamel, T. Stastny, K. Alexis, and R. Siegwart, "Model Predictive Control for Trajectory Tracking of Unmanned Aerial Vehicles Using Robot Operating System," in *Robot Operating System (ROS) The Complete Reference*. Springer, 2017, vol. 2.